

Quantum positioning and ranging via a distributed sensor network

Xiaocong Sun

Shanxi University

Wei Li

Shanxi University

Yuhang Tian

Shanxi University

Fan Li

Shanxi University

Long Tian

Shanxi University

Yajun Wang

Lab Quantum Optics & Quantum Optics Dev

Yaohui Zheng (✉ yhzheng@sxu.edu.cn)

Institute of Opto-Electronics, shanxi university <https://orcid.org/0000-0002-2231-951X>

Kunchi Peng

Shanxi University

Article

Keywords:

Posted Date: June 1st, 2022

DOI: <https://doi.org/10.21203/rs.3.rs-1659827/v1>

License:   This work is licensed under a Creative Commons Attribution 4.0 International License.

[Read Full License](#)

Quantum positioning and ranging via a distributed sensor network

Xiaocong Sun,^{1,*} Wei Li,^{1,2,*} Yuhang Tian,¹ Fan Li,¹ Long Tian,^{1,2} Yajun Wang,^{1,2} Yaohui Zheng,^{1,2,†} and Kunchi Peng^{1,2}

¹State Key Laboratory of Quantum Optics and Quantum Optics Devices, Institute of Opto-Electronics, Shanxi University, Taiyuan 030006, China

²Collaborative Innovation Center of Extreme Optics, Shanxi University, Taiyuan, Shanxi 030006, China

Abstract

Quantum sensor network with multipartite entanglement offers a sensitivity advantage in optical phase estimation over classical scheme. In order to tackle richer sensing problems, we construct a distributed sensor network with four nodes via four partite entanglements, unveil the estimation of the higher order derivative of radio-frequency signal phase, and unlock the potential of quantum target ranging and space positioning. Therefore, taking phased-array radar as an example, we demonstrate the optimal quantum advantages for space positioning and target ranging missions. Without doubt, the demonstration that endows innovative physical conception opens up a widespread application of quantum sensor network.

Introduction

Quantum metrology provides a route to conquer measurement sensitivity limitation imposed by quantum noise in sensing devices [1–3]. As a unique quantum resource, squeezed and entangled states present the feature of quantum correlation that can suppress statistical scaling of errors $n^{-\frac{1}{2}}$ in interferometric measurements, and thereby enhance measurement precision, until approaching and reaching to Heisenberg bound $1/n$ [4–6]. It holds particular relevance to power constraint introduced by optical damage or quantum measurement back-action, and ultra-weak signal that is thoroughly submerged into inherent quantum noise. Laser radar is one of the most prime cases of ultra-weak signal sensing, which has an urgent demand in measurement sensitivity beyond shot noise limit [7, 8].

Since quantum metrology was recognized in the 1980s [9], both the theoretical scheme and experimental technology of quantum metrology have advanced dramatically [10, 11]. In this regard, numerous demonstrations of quantum-enhanced metrology have been reported, for example, to enhance the performance of gravitational wave detection [12–15], magnetic field detection [16, 17], and biological measurement [18] and imaging [19, 20], as well are expected to be applied into more practical areas.

Furthermore, quantum sensing has been upgraded from a single sensor to a sensor network to realize spatially distributed sensing of multi-parameter. Theoret-

ical schemes of distributed quantum sensing have been proposed both in discrete variable (DV) domain [21–24] and continuous variable (CV) domain [25–29]. By utilizing entangled photons [30, 31] or entangled states [32], the average optical phase was estimated experimentally with a precision beyond what is achievable with separable probes. Very recently, Xia *et al.* extended the application of distributed quantum sensing to radio-frequency signal based on CV entanglement [33], and subsequently demonstrated the supervised learning assisted by an entangled sensor network for quantum-enhanced data classification [34]. However, taking a typical sensing mission for a phased array radar (PAR) as an example, the fundamental requirement is able to discover a target and acquires its position relative to the sensor, not only discriminates whether the target is present or not [35, 36]. The estimation of average phase shift is not enough to carry out mission mentioned above. In addition, the power limit of laser radar that comes from the endless pursuit of detecting range is ultimately determined by noise performance. For a classical system, the poor noise performance imposes restrictions on the intensity of return signal, and that in turn limits the detecting range, which has the potential to be improved to some extent via using squeezed light.

In this paper, we experimentally demonstrate quantum sensor network empowered by four-partite entanglement, optimizing quantum advantage in global parameter estimation including the higher order derivative of radio-frequency signal phase. The global parameter of four sensors $\varphi = \sum_{j=1}^4 \beta_j \varphi_j$, where β_j is the weights for different sensing problems, is estimated in our experiment, achieving quantum noise reduction of $6.0 \text{ dB} \pm 0.2 \text{ dB}$. Quantum sensor network is configured with an equally weighted distribution to maximize the quantum advantage for measuring the angle of arrival of the return signal along three independent dimensions, showing the quantum positioning. Sensor network is reconfigured with a weighted distribution of $-11/6$: 3 : $-3/2$: $1/3$ (2 : -5 : 4 : -1) to maximize the quantum advantage of the first (second) derivative of PAR phase, demonstrating quantum ranging.

PAR consists of multiple sensing elements appropriately arranged in space, whose amplitude and phase can be independently controlled to provide full space scanning without the influence of receiving sensitivity [37]. Space positioning can be realized by respectively measuring the angle of arrival of the return signal in three

*These authors contributed equally to this work

†Electronic address: yzheng@sxu.edu.cn

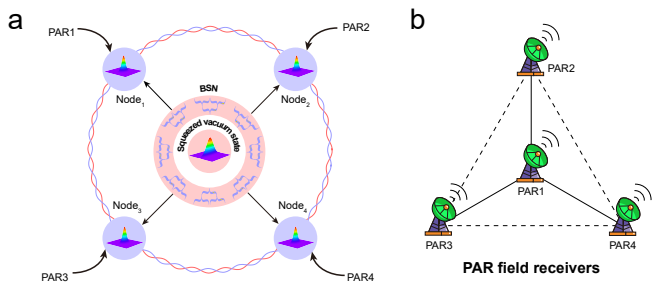


FIG. 1: **Schematic illustration of quantum positioning based on CV entangled network.** **a.** Principle of quantum positioning. **b.** Structural diagram of PAR network.

dimensions [38], which can be inferred from the phase difference between two sensor nodes of each dimension [33]. Thus, to achieve space positioning, it at least requires four sensor nodes. As the other key capacity, target ranging, dependent on the angle of arrival and its derivative of the return signal in one dimension, can be obtained by configuring a diverse weighted distribution among these sensor nodes. As such, a reconfigurable beam splitter network (BSN), in terms of minimum estimation variance, distributes the needed portion of squeezed state to these sensor nodes, leading to the optimal quantum advantage in different cases that serves as the estimation of the angle of arrival and its first (second) derivative beyond shot noise limit. There are two cases of sensor network topology: one is equilateral star topology for space positioning, and the other is linear topology for target ranging. Compared with the demonstration of only an average outcome among all of sensor nodes, the richer physics and more intriguing application scenario of distributed quantum sensor network are unveiled by our work.

Results

Quantum positioning protocol

Quantum positioning case: Three sensor nodes are arranged in an equilateral star topology, while the central node is situated at the triangle center, the schematic illustration of quantum positioning is represented in Fig. 1. When the target occurs, we can acquire three independent angles of arrival in three-dimensional space, and the target is positioned at the intersectional region of three angles of arrival. Critically, the distributed quantum sensor network must be optimized to generate minimum outcome uncertainty in a given distributed sensing problem. Here, to meet the requirement for simultaneous estimation of three angles of arrival with minimum positioning uncertainty, dependent on the phase difference between two sensor nodes with the function of $\theta = \arccos \frac{\lambda(\varphi_j - \varphi_1)}{2\pi\Delta x}$ ($j = 2, 3, 4$), a CV quantum sensor network with an equally weighted distribution is constructed. Under the circumstances, the additional noise coupling vanishes, leading to the minimum estimation

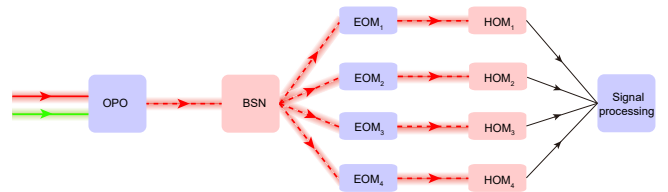


FIG. 2: **Experimental setup of quantum-enhanced PAR with a CV entangled network.** OPO: optical parametric oscillator; EOM: electro-optical modulator; HOM: homodyne detection.

variance of the PAR phase that depends on the initial squeezing factor. The equally weighted distribution is experimentally verified when the average variance for PAR phase $\varphi = \sum_{j=1}^4 \beta_j \varphi_j$ ($\beta_4 = \beta_3 = \beta_2 = 1, \beta_1 = -1$) reaches minimum. At this point, the uncertainties of three phase differences $\varphi_2 - \varphi_1$, $\varphi_3 - \varphi_1$ and $\varphi_4 - \varphi_1$ represent the best compromise, which look forward to having a boosted performance for target positioning.

A schematic illustration of our experimental setup is represented in Fig. 2. The squeezed state of light is generated by a below-threshold optical parametric oscillator (OPO), which has been shown in our previous publication in details [41]. The only difference is that our OPO operates at parametric amplification condition, leading to the generation of quadrature phase squeezed state. A BSN splits the state into four partite CV entangled states, which are used to sense the angle of arrival and the derivatives of arbitrary node, to realize quantum positioning and quantum ranging. Each sensor node entails an electro-optical modulator (EOM) to simulate the return signal from target, and a homodyne detection (HOM) to discern the return signal with the sensitivity beyond shot noise limit. The data are collected and postprocessed to derive the estimated parameters under different weights, and demonstrate diverse quantum-enhanced sensing applications.

The noise variances of measured PAR phase are limited by initial squeezing factor and system loss. It is worth noting that the parametric amplification process (for the generation of quadrature phase squeezed state) intensifies the noise coupling between the seed and pump field, which usually results in the degradation of the squeezing factor [42]. As the pump factor is increased, the noise coupling enhances. Thus, we need to make a trade-off between the pump factor and noise coupling, both of which are key factors of affecting the squeezing factor. Here, the OPO operates at the pump factor of $\sqrt{2}/2$, with quantum noise reduction of 8.0 ± 0.2 dB generated, providing superior quantum resource for the downstream experiment.

During the experiment, delicate mode-matching with interference efficiency of 99.8% is accomplished, the optimal weights are scheduled in terms of the different mission requirements, as well the number of optical elements is as few as possible, reducing the additional noise cou-

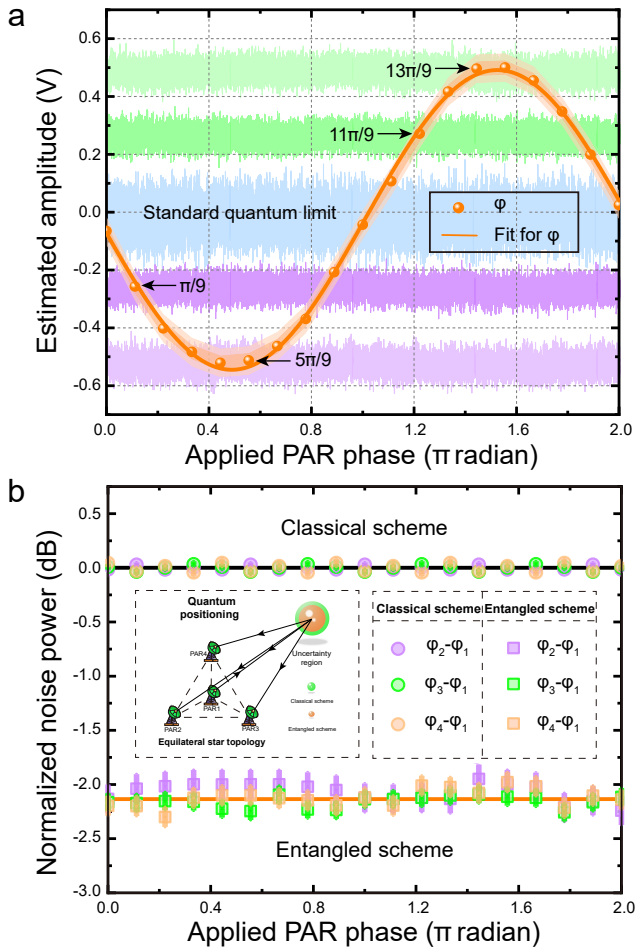


FIG. 3: **Estimation of average field amplitude and normalized noise powers versus applied PAR phases.** **a.** Estimated average field amplitude. Data points: average displacement from homodyne detection; orange curves: a sinusoidal fit; orange shaded area: estimation uncertainties for the entangled (dark color) and classical separable (light color) sensor networks. The blue curve shows the time-domain measurement result of standard quantum limit, the purple, light purple, green, and light green curves represent the measurement results with entangled sensor network at several PAR phase ($\pi/9$, $5\pi/9$, $11\pi/9$ and $13\pi/9$). **b.** Measured noise powers of three phase differences. Black and orange curves show the noise powers based on classical and entangled scheme, respectively. The circular and square data points represent noise powers of three different phase differences with classical and entangled scheme, respectively. All measurement results are normalized to the standard quantum limit.

pling to the maximum extent, minimizing the estimation variance of diverse physical scenarios. On the other hand, the phase of demodulation signal is carefully optimized to suppress the noise coupling of anti-squeezing quadrature into squeezing quadrature as much as possible.

Suppose that the PAR operates in single-transmitter and multi-receivers mode, we show the experimental results of quantum-enhanced PAR in two sensing tasks.

The PAR1 serves as transmitter and receiver, all the other nodes act as receivers.

Under ideal conditions, three angles of arrival define a point in space, which is the principle of target positioning [39]. However, the quantum noise of optical field imposes a limitation on the positioning precision, defining a space region, instead of a point. The positioning precision can be improved by reducing the estimation variance of each angle of arrival. According to the above analysis, a quantum sensor network with an equally weighted distribution can offer a precision advantage in the angle of arrival estimation over with other weighted one. We estimate the average displacement for radio-frequency phase ($\varphi = \varphi_4 + \varphi_3 + \varphi_2 - \varphi_1$) by measuring the phase quadrature of each node and summing the photocurrents of four HOMs. Fig. 3(a) represents the estimation of average field amplitude and estimation variance for φ as a function of the applied PAR phases for all sensors synchronously. By minimizing the estimation variance, a $6.0 \text{ dB} \pm 0.2 \text{ dB}$ quantum noise reduction is achieved, confirming the entanglement properties of sensor network with equal weighted distribution. At this point, the splitting ratios of three variable beam splitters (VBSs) are 25:75, 33:67 and 50:50, respectively, the three angles of arrival are quantified. Fig. 3(b) shows the measured noise powers for three phase differences $\varphi_j - \varphi_1$ ($j = 2, 3, 4$) for estimating angle of arrival at different applied PAR phases. The measurement noise variances of three phase differences, represented by purple, green, and orange, are plotted for both quantum (square) and classical (circle) cases. The estimation variances for several cases are normalized to the shot noise limit. It is evident that quantum-enhanced sensor network leads to a reduction in the estimation variance, whereas such a noise reduction mechanism is absent without the quantum resource. The reduced noise powers of $-2.1 \pm 0.1 \text{ dB}$ for $\varphi_2 - \varphi_1$, $-2.2 \pm 0.1 \text{ dB}$ for $\varphi_3 - \varphi_1$ and $-2.1 \pm 0.1 \text{ dB}$ for $\varphi_4 - \varphi_1$ are obtained, which means, the detection range is expanded by at least 12.8% [39]. The noise variances are independent of the applied PAR phases, allowing the realization of 360-degree arbitrary scanning. The inset of Fig. 3(b) shows the principle of the improved positioning precision. It can be inferred that the uncertainty region of our protocol with multipartite entanglement is reduced to 0.4837 in three-dimensional space, in contrast with classical protocol, corresponding to the positioning precision improvement of 51.6%.

Quantum ranging protocol

Quantum ranging case: Except for target positioning, target ranging is another critical specification of radar system, which can be expressed as [39]

$$r = \frac{(\varphi'_1)^2}{\varphi''_1} \frac{\lambda}{36\pi\Delta x} (-\sin \zeta x' - \cos \zeta y' + iz'), \quad (1)$$

where φ'_1 and φ''_1 are the first and second derivatives of the edge node PAR1, λ is the wavelength of the PAR

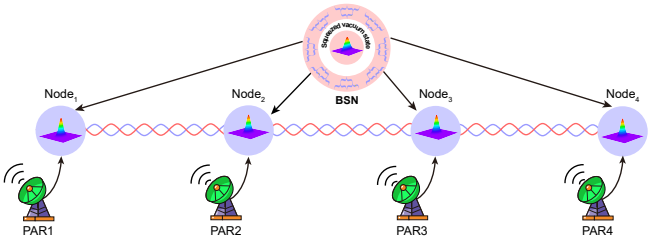


FIG. 4: Schematic illustration of quantum ranging based on CV entangled network.

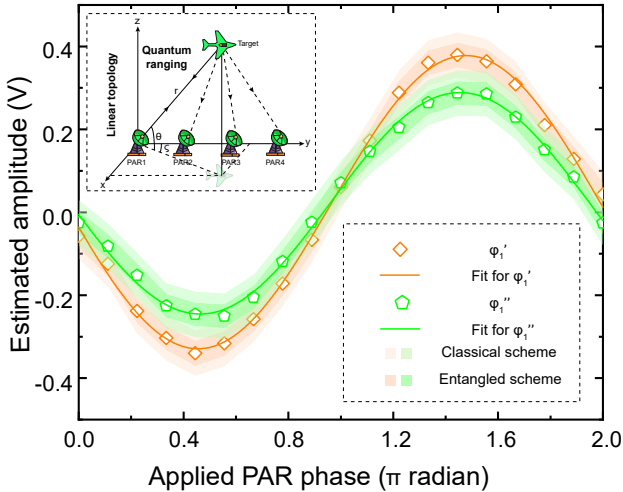


FIG. 5: Comparison of the estimated amplitude for the first and second derivatives of the PAR phase under two cases. Data points: the means of the measured homodyne signals; curves: the sinusoidal fit; shaded area: estimation uncertainties for the entangled (dark color) and classical separable (light color) sensor networks. All signals are normalized using the same factor for the standard quantum limit normalization.

field, Δx indicates the distance between each two sensors, x' , y' and z' show the movement speed of target, ζ represents azimuth angle of target in terms of PAR plane. The azimuth angle ζ can be obtained from positioning case demonstrated in the previous paragraph. According to the Eq. 1, the target ranging can be transferred to the estimation of the first and second derivatives of edge node PAR1. Exploiting the Taylor series expansion of phase estimator with the estimated phase φ_1 of edge node PAR1, the optimum weights for the first and second derivatives are expressed as $\beta_1 : \beta_2 : \beta_3 : \beta_4 = -11/6 : 3 : -3/2 : 1/3$ and $2 : -5 : 4 : -1$, respectively [39]. As the number of the nodes increases, higher-order derivatives for edge node PAR1 can be obtained, standing for richer physical scenario. Here, as shown in the inset of Fig. 4, four sensor nodes are arranged along a straight line, the edge node PAR1 serves as a reference.

To achieve the optimum performance in quantum ranging, weighted distributions need to be configured on the

grounds of physical quantity measured. At the same time, the PAR network is arranged in a linear topology. The optimal weight $-11/6 : 3 : -3/2 : 1/3$ ($2 : -5 : 4 : -1$) is arranged to implement the minimum estimation variance of the first (second) derivative of edge node PAR1, thereby the splitting ratios of the VBSs are corresponding to 27.5:72.5, 62:38 and 82:18 (17:83, 50:50 and 80:20) respectively [39]. The negative signs in the weights are introduced by adding a π -phase delay in the corresponding optical path. Fig. 5 shows the estimated average amplitude of the first and second derivatives of PAR1 as a function of applied PAR phase, with shaded area region representing the estimation uncertainty of the first (second) derivative of the node, deep orange (green) for quantum sensing protocol, light orange (green) for classical protocol. In order to satisfy 360-degree fast scanning, a precision advantage of quantum ranging should be offered at arbitrary azimuth angle, irrespective of applied PAR phase. Compared with the classical protocol, the almost invariable noise reductions of -5.0 ± 0.1 dB for the first derivative and -5.4 ± 0.2 dB for the second derivative are implemented in the experiment, demonstrating the full scanning range with enhanced precision. The inset of Fig. 5 represents the topology structure of quantum ranging. In addition, the noise suppression in three independent relative phase differences, the first and second derivatives of edge node is still maintained when the applied PAR amplitude varies, which confirms that the PAR network can be compatible with the return signal with different intensity without sacrificing its precision [39]. It can be inferred from the results of Fig. 5 that the pitch angle with enhanced precision of 68.4% is achieved on all-round scanning. Furthermore, combining with the noise suppression of 5.4 dB for φ_1' , the target ranging with enhanced precision of 69.3% can be realized. In other words, with the same signal to noise ratio (SNR) of return signal, the detection range of radar is increased by 34.3%. It is worth noting that quantum ranging can be realized only when both the first and second derivatives are measured simultaneously, meaning that at least three sensor nodes in line are required. In combination with quantum ranging, the space positioning of target becomes more accurate.

Conclusion

In conclusion, we have implemented the demonstration of quantum-enhanced PAR network exploiting CV multipartite entanglement state, verifying the feasibility of quantum positioning and quantum ranging. By utilizing sensor network with an average weighted distribution, quantum positioning offers a precision advantage of 51.6% in three-dimensional space over classical scheme, increasing the detection range by 12.8%. Moreover, in virtue of diverse weighted distributions, quantum ranging with enhanced precision of 69.3% can be realized, thus the detection range of radar is increased by 34.3% with the same signal to noise ratio (SNR) of return signal. We expect to construct a distributed sensing net-

work via multipartite entanglement state, which can simultaneously achieve quantum positioning and ranging in combination with two cases proposed by this article. Moreover, the universal distributed quantum sensing proposal can easily be extended to other applications including target tracking, off-axis digital holograms, and phased array sonar [44, 45].

Methods

The experimental setup is divided into three parts: generation of phase squeezed state, RF sensor network and data acquisition. The squeezed state is generated by a sub-threshold optical parametric amplifier (OPA) that is composed by a PPKTP crystal and a piezo-actuated output coupler. One face of PPKTP crystal has the dimension of 1 mm*2 mm*10 mm and a radius of curvature of 12 mm, while the other face is a flat surface with AR-coating. The convex face of crystal has highly reflective (HR) coating for 1064 nm and anti-reflective coating for 532 nm, whereas the output coupler has transmissivity of 12% for 1064 nm and HR coating for 532 nm. The radius of curvature for output coupler is 30 mm, and the air gap between crystal and output coupler is about 27 mm. It is worth mentioning that the relative phase between the fundamental and harmonic fields is locked to zero, generating the phase squeezed state.

The PAR sensor network consists of entangled net-

work, EOMs and HOMs. With the phase squeezed state, four partite CV entangled states are generated by a BSN that is composed of three pairs of half-wave plates (HWPs) and polarization beam splitters (PBSs). The BSN can be set to any splitting ratio. The EOM that has high radio-frequency to photonics conversion efficiency, is an excellent simulator of PAR. Four EOMs are independently driven by four clock-synchronized function generators with the same modulation frequency of 3 MHz, but the amplitude and phase are independently manipulated to generate four independent displacements α_j ($j = 1, 2, 3, 4$) on the squeezed phase quadrature [33]. In each HOM node, the relative phase between local oscillator and sensing beam is controlled to $\pm \frac{\pi}{2}$ by utilizing the interference signal as error signal. In data acquisition state, the output of four HOMs through four same band-pass filters from 1.8 MHz to 4.5 MHz is demodulated with 3 MHz signals, respectively. The demodulation signals are clock synchronized with the corresponding return signals, but their phases can be independently manipulated to compensate the delay difference of the processing circuit. The time-domain data from four mixers are collected and postprocessed to derive the estimated parameters under different weights, and demonstrate diverse quantum-enhanced sensing applications.

References

- [1] V. Giovannetti, S. Lloyd, & L. Maccone, Advances in quantum metrology, *Nat. Photon.* **5**, 222 (2011).
- [2] V. Giovannetti, S. Lloyd, & L. Maccone, Quantum Metrology, *Phys. Rev. Lett.* **96**, 010401 (2006).
- [3] L. Pezzè, A. Smerzi, M. K. Oberthaler, R. Schmied, & P. Treutlein, Quantum metrology with nonclassical states of atomic ensembles, *Rev. Mod. Phys.* **90**, 035005 (2018).
- [4] M. Zwiernik, C. A. Pérez-Delgado, & P. Kok, General optimality of the Heisenberg limit for quantum metrology, *Phys. Rev. Lett.* **105**, 180402 (2010).
- [5] V. Giovannetti, S. Lloyd, & L. Maccone, Quantum-enhanced measurements: Beating the standard quantum limit, *Science* **306**, 1330 (2004).
- [6] B. Escher, R. M. Filho, & L. Davidovich, General framework for estimating the ultimate precision limit in noisy quantum-enhanced metrology, *Nat. Phys.* **7**, 406 (2011).
- [7] Q. Zhuang, Z. Zhang, & J. H. Shapiro, Entanglement-enhanced lidars for simultaneous range and velocity measurements, *Phys. Rev. A* **96**, 040304(R) (2017).
- [8] L. Maccone, & C. Ren, Quantum Radar, *Phys. Rev. Lett.* **124**, 200503 (2020).
- [9] C. M. Caves, Quantum-mechanical noise in an interferometer, *Phys. Rev. D* **23**, 1693 (1981).
- [10] S. Slussarenko, M. M. Weston, H. M. Chrzanowski, L. K. Shalm, V. B. Verma, S. W. Nam & G. J. Pryde, Unconditional violation of the shot-noise limit in photonic quantum metrology, *Nat. Photon.* **11**, 700 (2017).
- [11] D. Braun, G. Adesso, F. Benatti, R. Floreanini, U. Marzolino, M. W. Mitchell, & S. Pirandola, Quantum-enhanced measurements without entanglement, *Rev. Mod. Phys.* **90**, 035006 (2018).
- [12] R. Schnabel, N. Mavalvala, D. E. McClelland, & P. K. Lam, Quantum metrology for gravitational wave astronomy, *Nat. Commun.* **1**, 121 (2010).
- [13] The LIGO Scientific Collaboration, A gravitational wave observatory operating beyond the quantum shot-noise limit, *Nat. Phys.* **7**, 962 (2011).
- [14] M. Tse *et al.*, Quantum-Enhanced Advanced LIGO Detectors in the Era of Gravitational-Wave Astronomy, *Phys. Rev. Lett.* **123**, 231107 (2019).
- [15] The LIGO Scientific Collaboration, Enhanced sensitivity of the LIGO gravitational wave detector by using squeezed states of light, *Nat. Photon.* **7**, 613 (2013).
- [16] B. Li, J. Bílek, U. B. Hoff, L. S. Madsen, S. Forstner, V. Prakash, C. Schäfermeier, T. Gehring, W. P. Bowen, & U. L. Andersen, Quantum enhanced optomechanical magnetometry, *Optica* **5**, 850 (2018).
- [17] F. Wolfgang, A. Cerè, F. A. Beduini, A. Predojević, M. Koschorreck, & M. W. Mitchell, Squeezed-Light Optical Magnetometry, *Phys. Rev. Lett.* **105**, 053601 (2010).
- [18] M. Taylor, J. Janousek, V. Daria, J. Knittel, B. Hage, H. Bachor, & W. P. Bowen, Biological measurement beyond the quantum limit, *Nat. Photon.* **7**, 229 (2013).
- [19] C. A. Pérez-Delgado, M. E. Pearce, & P. Kok, Fundamental limits of classical and quantum imaging, *Phys. Rev. Lett.* **109**, 123601 (2012).
- [20] G. H. Low, T. J. Yoder, & I. L. Chuang, Quantum Imaging by Coherent Enhancement, *Phys. Rev. Lett.* **114**, 100801 (2015).

- [21] W. Ge, K. Jacobs, Z. Eldredge, A. V. Gorshkov, & M. Foss-Feig, Distributed Quantum Metrology with Linear Networks and Separable Inputs, *Phys. Rev. Lett.* **121**, 043604 (2018).
- [22] P. C. Humphreys, M. Barbieri, A. Datta, & I. A. Walmsley, Quantum Enhanced Multiple Phase Estimation, *Phys. Rev. Lett.* **111**, 070403 (2013).
- [23] T. J. Proctor, P. A. Knott, & J. A. Dunningham, Multiparameter Estimation in Networked Quantum Sensors, *Phys. Rev. Lett.* **120**, 080501 (2018).
- [24] Z. Eldredge, M. Foss-Feig, J. A. Gross, S. L. Rolston, & A. V. Gorshkov, Optimal and secure measurement protocols for quantum sensor networks, *Phys. Rev. A* **97**, 042337 (2018).
- [25] Q. Zhuang, Z. Zhang, & J. H. Shapiro, Distributed quantum sensing using continuous-variable multipartite entanglement, *Phys. Rev. A* **97**, 032329 (2018).
- [26] C. Oh, C. Lee, S. H. Lie, & H. Jeong, Optimal distributed quantum sensing using Gaussian states, *Phys. Rev. Research* **2**, 023030 (2020).
- [27] Q. Zhuang, J. Preskill, & L. Jiang, Distributed quantum sensing enhanced by continuous-variable error correction, *New J. Phys.* **22**, 022001 (2020).
- [28] S. Pirandola, B. R. Bardhan, T. Gehring, C. Weedbrook & S. Lloyd, Advances in photonic quantum sensing, *Nat. Photon.* **12**, 724 (2018).
- [29] Q. Zhuang & Z. Zhang, Physical-Layer Supervised Learning Assisted by an Entangled Sensor Network, *Phys. Rev. X* **9**, 041023 (2019).
- [30] L. Liu, Y. Zhang, Z. Li, R. Zhang, X. Yin, Y. Fei, L. Li, N. Liu, F. Xu, Y. Chen & J. Pan, Distributed quantum phase estimation with entangled photons, *Nat. Photon.* **15**, 137 (2021).
- [31] S. Zhao, Y. Zhang, W. Liu, J. Guan, W. Zhang, C. Li, B. Bai, M. Li, Y. Liu, L. You, J. Zhang, J. Fan, F. Xu, Q. Zhang, & J. Pan, Field Demonstration of Distributed Quantum Sensing without Post-Selection, *Phys. Rev. X* **11**, 031009 (2021).
- [32] X. Guo, C. R. Breum, J. Borregaard, S. Izumi, M. V. Larsen, T. Gehring, M. Christandl, J. S. Neergaard-Nielsen & U. L. Andersen, Distributed quantum sensing in a continuous-variable entangled network, *Nat. Phys.* **16**, 281 (2020).
- [33] Y. Xia, W. Li, W. Clark, D. Hart, Q. Zhuang, & Z. Zhang, Demonstration of a Reconfigurable Entangled Radio-Frequency Photonic Sensor Network, *Phys. Rev. Lett.* **124**, 150502 (2020).
- [34] Y. Xia, W. Li, Q. Zhuang, & Z. Zhang, Quantum-Enhanced Data Classification with a Variational Entangled Sensor Network, *Phys. Rev. X* **11**, 021047 (2021).
- [35] V. Giovannetti, S. Lloyd, and L. Maccone, Positioning and clock synchronization through entanglement, *Phys. Rev. A* **65**, 022309 (2002).
- [36] V. Giovannetti, S. Lloyd, and L. Maccone, Quantum-enhanced positioning and clock synchronization, *Nature* **412**, 417 (2001).
- [37] J. W. Zang, A. Alvarez-Melcon, and J. S. Gomez-Diaz, Nonreciprocal Phased-Array Antennas, *Phys. Rev. Applied* **12**, 054008 (2019).
- [38] P. Kułakowski, J. Vales-Alonso, E. Egea-López, W. Ludwin, & J. García-Haro, Angle-of-arrival localization based on antenna arrays for wireless sensor networks, *Comput. Electr. Eng.* **36**, 1181 (2010).
- [39] See Supplemental Material at [URL will be inserted by publisher], which includes Refs. [33, 38, 40], for principle of space positioning, theoretical model of the quantum ranging, calculation of optimum weights, additional experimental results, dependence of entanglement on beam splitter ratio and detection range of radar.
- [40] K. Langendoen, & N. Reijers, Distributed localization in wireless sensor networks: a quantitative comparison, *Comput. Netw.* **4**, 499 (2003).
- [41] S. Shi, L. Tian, Y. Wang, Y. Zheng, C. Xie, & K. Peng, Demonstration of channel multiplexing quantum communication exploiting entangled sideband modes, *Phys. Rev. Lett.* **125**, 070502 (2020).
- [42] X. Sun, Y. Wang, L. Tian, S. Shi, Y. Zheng, & K. Peng, Dependence of the squeezing and anti-squeezing factors of bright squeezed light on the seed beam power and pump beam noise, *Opt. Lett.* **44**, 1789 (2019).
- [43] I. S. Merrill, Introduction to radar systems, Mc Grow-Hill **7** (2001).
- [44] Q. Zhuang, Quantum Ranging with Gaussian Entanglement, *Phys. Rev. Lett.* **126**, 240501 (2021).
- [45] C. Guo, B. Wang, B. Sha, Y. Lu, & M. Xu, Phase derivative method for reconstruction of slightly off-axis digital holograms, *Opt. Express* **22**, 30553 (2014).

Acknowledgements

The authors acknowledge financial support from the National Natural Science Foundation of China (NSFC) (Grants No. 62027821, No. 11654002, No. 11874250, No. 11804207, No. 11804206, No. 62035015 and No. 12174234); National Key R&D Program of China (Grant No. 2020YFC2200402); Key R&D Program of Shanxi (Grant No. 201903D111001); Program for Sanjin Scholar of Shanxi Province.

Author contributions

X.S. and W.L. performed the experiment and analyzed the data. Y.T. and F.L. contributes to the data collection. Y.W. and L.T. developed ideas for both implementing methods and which physics to study. Y.Z. and K.P. supervised all work, as well as contributed to deciding the experiment scheme and processing the data, and setting up the physical models. All authors discussed the results and contributed to the manuscript.

Additional information

Competing interests The authors declare no competing interests.

Correspondence and requests for materials should be addressed to Y. H. Z. (email: yhzhang@sxu.edu.cn).

Data availability

The data sets generated and/or analyzed during the current study are available from the corresponding author on reasonable request.

Supplementary Files

This is a list of supplementary files associated with this preprint. Click to download.

- [SupplementaryInformation.pdf](#)